2-28-2019

The Selection of Parameters in Debris Flow Modeling: A Sensitivity Study Using the Discrete Element Method

Cora Siebert
Portland State University

The Selection of Parameters in Debris Flow Modeling: A Sensitivity Study Using the Discrete Element Method

Cora Siebert

February 28, 2019

Abstract

Many studies have examined runout behavior of debris flows on various slopes and in different environments, but few have explicitly modeled their coarse woody debris component. Simulating a coarse-grained debris flow snout including coarse woody debris can be achieved using discrete element modeling. Before modeling the entire system, each parameter that influences the model must be determined and analyzed. Using 5 m resolution IfSAR data from Sitka, Alaska as the control topography, I conducted a sensitivity analysis of the behavior of a single particle as it travels downslope. Parameters of relevance are normal and tangential contact stiffness, viscous damping coefficient, and friction coefficient. Each parameter influences the amount of time that the particle spends in the air (i.e., making no contact with the topography), with stiffness and damping parameter being the most influential parameters on time spent in the air. For future work, using parameter values of 9.5e8 N/m for normal contact stiffness, 4.8e11 N/m for shear contact stiffness, a viscous damping coefficient of 0.8, and a friction coefficient of 0.6 to simulate boulders with a density of 2600 kg/m^3 and radius of 5.0 meters should be optimal for simulating debris flow dynamics of the coarse-grained snout. Finally, with appropriately behaving sediment, coarse woody debris may be included in the model and the system can be observed.

Introduction

In mountainous, forested terrain, debris flows play a primary role in exporting sediment and woody debris from their original location. Debris flow mechanics have been widely studied, but few studies have analyzed the role of coarse woody debris (CWD) as it affects runout length. Such an analysis is essential for understanding debris flow mechanics because CWD can be more than half the volume fraction of a flow's composition. Granular effects such as jamming of CWD along with the uneven surface of the topography affects the frictional resistance of the debris flow as a whole, thus influencing several important aspects of flow mechanics. Providing an analysis of the relationship between CWD and runout length allows for further investigation of the relationship between topographical dynamics and ecosystem evolution. The purpose of this study is to explore the parameters necessary to realistically model granular flows.

Literature Review

Landslides, which can mobilize into debris flows, occur when the shear strength of a potential failure plane falls below the shear stress of the coplanar mass. During such a failure, surrounding organic material and CWD may be entrained and transported away from their original location, thus altering the debris flow's original composition and behavior. Runout lengths can therefore be affected by forest age or landscape characteristics. For example, in a study performed at the central Oregon Coast Range it was found that runout length of debris flows was longest for those that initiated at roads, as opposed to those that initiated in mature forests (29% of the basin areas for that study). Those initiated at roads lacked significant volumes of CWD and traveled 3.1 times farther (May, 2002). It was shown that, because larger debris flows entrain more CWD, the volume of wood in debris flow deposits was correlated with the cumulative runout length of the debris flow path, and debris flows through mature forests had the highest volume of wood per unit length of runout (May, 2002). In this same study, it was found that the diameter of the CWD in the deposit was larger than the trees currently present on surrounding hillslopes in clearcuts, 46% of the total number of landslides observed, and second growth forests, indicating that they were transported from more mature forests into a younger forest. Of the debris flow deposits studied, an entire half of their volumes were from entrainment during runout (May, 1998). In a similar study performed in SE Alaska, it was found that landslide deposits in old-growth forest contained between 10% and 35% CWD, typically holding ten times the woody debris volume of deposits originating in clearcuts (Johnson et al., 2000). Higher depositional slopes may correspond to increased woody debris content (Johnson et al., 2000). Although woody debris volume has been qualitatively accounted for in previous studies, a quantitative approach to this problem

could offer insight to the runout aspect of debris flow mechanics.

To date, very few studies have explicitly modeled CWD in debris flows. One of the most advanced models treats debris flow motion as a one-dimensional point process, where that point moves with the front of the flow, and velocity and depth are functions of time (Lancaster et al., 2003). CWD was incorporated in two ways: bends in the channel, where CWD tends to jam and create a block, and entrainment of the CWD into the debris mixture. Because of the way a debris flow "bulldozes" and entrains surface wood, an algorithm was implemented that forces a flow to stop if enough wood to overcome the momentum of the flow is present. This algorithm uses the equation for conservation of momentum, allowing a simulated flow to stop, thereby providing runout length. The equation for conservation of momentum is

$$\frac{d}{dt}(\rho h v) = (\text{-sgn}v)(\rho h g \cos\theta - p_b)\left(1 + \frac{v^2}{g\cos\theta}\frac{d\theta}{ds}\right)\tan\phi_b + \rho g h \sin\theta \tag{1}$$

where h is slope-normal debris flow depth; v is slope-parallel debris flow velocity; t is time; p_b is pore pressure at the bed; ρ is debris flow mixture density which is updated at every time step from the relative proportions and densities of the constituents (sediment, water, and wood); s is the distance in the slope-parallel direction; $\phi_b$is bed friction angle; θ is the slope angle of the ground beneath the flow; g is acceleration due to gravity; and the factor -sgn indicates the direction opposite that of debris flow velocity (Lancaster et al., 2003). Changes in density and depth result from the entrainment of wood, sediment, and water, as well as changes in valley geometry. Several terms are neglected (e.g., convective accelerations; longitudinal normal stresses that characterize interaction between debris flow head and tail; multidimensional momentum transfers arising from the fact that velocity is a vector quantity, etc.) for feasibility (Lancaster et al., 2003).

Broken down into terms, $(\rho g h \cos\theta - p_b)$ describes the static effective normal stress, $(1 + \frac{v}{g\cos\theta}\frac{d}{ds})$ indicates radial acceleration including centripetal acceleration for going over humps in the topography, which modifies the effective normal stress, and multiplying these terms by $\tan\phi_b$ gives the frictional strength of the debris flow. The last term, $\rho g h \sin\theta$ is the driving stress, which is theproduct of mass and gravity for the slope angle. Debris flow entrainment can be modeled through considering the minimum depth of bed material that will fail after being provided the "overburden of a debris flow in motion" (Lancaster et al., 2003). Similar to the physics of land failure, sediment entrainment occurs when scouring takes place, or when the net impelling stress is greater than the sum of the resisting and impelling stresses (Lancaster et al., 2003).

In the model introduced above, interpolated and gridded digital elevation model data is used to create a

reasonable topography, where nodes are set at specific elevations in a triangular irregular network (TIN). Edges of the nodes are connected, creating a Voronoi area. Some changes to the TIN are occasionally made, such as adding nodes to drainage areas in order to reduce "jaggedness" common with interpolated data. Nodes may then be classified as hillslope, channel, and valley nodes (Figure 1). Properties and behavior of the debris flow can be calculated at each node, using changes in depth, density, and width to update Equation 1 for a change in velocity due to momentum conservation.

While running the model, as a debris flow approaches and hits a new node, the velocity reduction due to bend angle must be calculated. Because 1 is dependent on rate of depth and density change, these must be determined beforehand. Next, depth, density, velocity, and position are recorded at each time step until the flow reaches the current flow edge, or velocity has reached zero (indicating that the debris flow has stopped). While this model produces reasonable runout behavior for debris flows with CWD, it doesn't take into account the interactions of each sediment particle with another, as well as the interactions of CWD with each sediment particle, which may allow for a much more realistic model that encompasses a larger portion of the system.

Discrete element modeling is a quantitative approach that focuses on the interaction of individual particles within a modeled system, and has been used in the areas of soil and rock mechanics to study the load behavior of such materials (Chen and Matuttis, 2014). Although DEM does not include the effects of water, it is relevant to the mechanics of the debris flow snout where pore pressures are often near zero and solid stresses dominate behavior. The choice of particle shape is crucial to the accuracy of a model, and must be treated with care. Particle shape, size, density, and elastic and frictional properties will allow explicit simulation of CWD in a debris flow while being able to retrieve data about each particle at every time step. Such an analysis method has been implemented for the study of landslide hazard forecasting, kinematic modeling, sediment mixing, among many more applications (Lo et al., 2011a; Lu et al., 2014; Mishra et al., 2002).

The discrete element method (DEM) was used, for example, to study landsliding behavior after the 1999 Chi-Chi earthquake in Taiwan. Within this study, research into the apparent friction coefficient of the Tsaoling landslide, a massive catastrophic long runout landslide with a volume of 125×10^6 m^3 (Hung et al., 2002), was able to be completed. Defined as the ratio between the total vertical and horizontal displacements of the center of mass, landslides of this type have a smaller apparent friction coefficient than that provided by standard tests of material mechanical properties (Tang et al., 2009). An apparent friction coefficient is equal to the friction coefficient under several conditions: 1) that the friction coefficient is constant during motion, 2) the loss of kinetic energy by the landslide is caused only by frictional resistance, and 3) the

landslide pathway is the minimum path (of Fluid Mechanics). By using the discrete element method, they were able to represent the kinematics and mechanical behavior of the Tsaoling landslide as constrained by the geometry and structure of the sliding mass, both before and after the event (Tang et al., 2009).

This undergraduate thesis focuses on defining the relevant material parameters for discrete element modeling to simulate debris flow runout, using the surrounding topography of Sitka, Alaska, USA as the reference topography. A large storm event occured in Sitka in 2015 where over 10 cm of rain fell in under 4 hours, resulting in more than 40 mapped landslides. To first create these models, tests must be performed to determine appropriate parameters for calibrating the system. Presented here are such calibration tests for a representative debris flow channel in the study area.

Research Questions and Hypothesis

A study of this magnitude must begin with an exploration of the importance of the system's parameters. These parameters include particle radius, density, normal and shear contact stiffness, friction coefficient, and viscous damping ratio. The effect of stiffness, friction coefficient, and viscous damping ratio on the system, with radius and density held constant, will be explored, answering the questions "which parameters have the greatest effect on a granular flow model?" and "what parameter values produce realistic behavior?"

I hypothesized that the effect of the damping coefficient would have the biggest impact on the system because of its use in energy dissipation in DEM. This energy dissipation would have a large effect on the interaction between the particle, also referred to as the "ball," and the topography. I believed that if I increased the damping coefficient the amount of time the particle spent in the air would linearly decrease, producing more realistic debris flow behavior since they rarely leave the ground and become airborne.

Research Methods

The hypothesis was tested by sending one particle down a slope using Particle Flow Code 3D (PFC3D), an advanced multi-physics simulation software specifically for modeling using the Discrete Element Method. DEM is an appropriate approach for a debris flow mechanics study due to its ability to simulate thousands of particles and provide data on the particle-scale level. In other words, it provides a microscopic understanding of macroscopic particulate material behavior. Although a critical component of debris flow mechanics is the liquified debris flow tail, the goal of this study is to give undivided attention to the role of friction in the system at the debris flow snout where solid forces dominate. Once reliable 'dry' models have been developed, the addition of water (among other external impacting forces) may be considered. This allows

for a more specific examination of the jamming and locking of CWD and changes in friction coefficient at different portions of the debris flow.

Discrete element modeling is made possible by specifying all external forces on each particle assuming they behave as a mass-spring-dashpot system. With these forces explicitly defined, integration of Newton's laws of motion reveals particle behavior at each time step. The classical equation for a mass-spring-dashpot system is

$$m\frac{\mathrm{d}^2\delta}{\mathrm{d}t^2} + \eta\frac{\mathrm{d}\delta}{\mathrm{d}t} + k_L\delta = 0 \tag{2}$$

where m is the mass of the particle, k_L is the linear-spring constant or stiffness, δ is the overlap between the particle and the topography, and η is the damping coefficient. The damping coefficient can only be applied to cases where $\eta \geq 0$ because the contact force is only active when the particle is in contact with its base (Malone and Xu, 2008).

Contact stiffness is a parameter that plays a large role in how particles interact with each other and their topography. By setting this parameter, compliance, the ratio of strain to stress, can be incorporated into the model. Considering two spheres of random radii being pushed toward one another, they are allowed to overlap by a set amount. Subtracting the distance between the two sphere's centers from the sum of the radii offers a value that can be controlled with the contact stiffness parameter. As interpreted by Malone et al (2011), contact stiffness considered the impact velocity, v_i, and the resulting overlap, δ, by

$$k_L = \frac{mv_i^2}{\delta_{v_i}^2}. \tag{3}$$

Viscous damping is incorporated into the model in the normal direction and contributes to the consumption of system energy (Malone and Xu, 2008). As interpreted by Navarro et al, one will often use the coefficient of restitution, defined as

$$e = \frac{v_1}{v_0}, \tag{4}$$

where e is the coefficient of restitution, and v_0 and v_1 are the components of relative velocity at the contact point before and after the collision for each colliding particle (Malone and Xu, 2008), as a basis for determining an appropriate contact stiffness. The coefficient of restitution is typically between zero and 1, where one is a perfectly elastic collision. This value may also be calculated by

$$e = \sqrt{\frac{h_1}{h_0}}, \tag{5}$$

where h_0 is the height that the particle was dropped from and h_1 is the height to which it rebounds after colliding with the base (Malone and Xu, 2008). Equations 4 & 5 can be used, along with a predetermined particle material, size, and drop height, to determine a suitable damping coefficient. In the case of this study, however, none of those properties can be acquired and hence, the damping coefficient is tested at various values to explore its impact on the system.

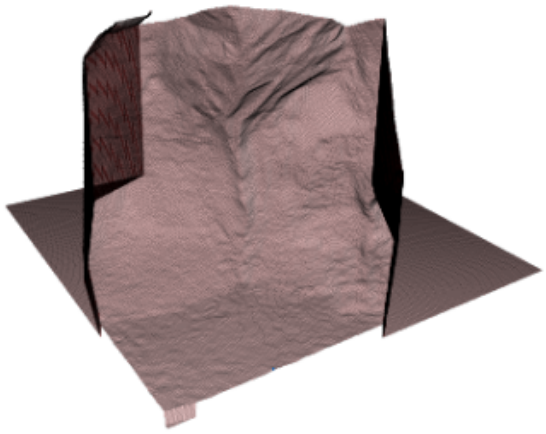

Figure 1: IfSAR derived digital elevation model used throughout the following tests as seen within PFC3D.

The interactions between each particle will be controlled by defining particle size, geometry, density, contact stiffness, and damping constant. By default, particles are always spheres with a chosen diameter, however, with the PFC3D's newly implemented 'clump logic', spheres of various sizes are 'clumped together' to create realistic CWD. This allows for excellent control over hillslope sediment soil composition and sorting, as well as CWD length, diameter, and profile.

To conduct the sensitivity analysis, each parameter was varied while holding the others constant at values used by Lo et al (2011a) in a study that modeled the Hsiaolin landslide, a deadly landslide resulting from Typhoon Morakot in 2009.

Parameters chosen for their study were determined based on a series of compression numerical tests on granular samples to derive rock mechanical macro-properties of the granular assembly (Lo et al., 2011b).

In the present study, the default parameters can be seen in 1, and the ranges tested in 2. Tests were taken for two different types of trials that are exactly similar except for the particle's starting location. This was to assess the influence of initial conditions on subsequent behavior. The two starting locations are spaced 5 meters apart from each other, and the contact force experienced by the topography as well as elevation of the particle as a function of time is collected to compare different model runs.

The model domain and boundary conditions (Figure 1) came from a Digital Elevation Model (gathered by IfSAR) at 5m resolution. Within the GIS system, digital elevation data was prepared using the TIN format previously mentioned (see Introduction).

While models were being run within PFC3D, data was collected for the particle's position, velocity, contact force, and kinetic energy, each of which was output by FISH, an embedded programming language within PFC3D (Chen and Matuttis, 2014). Initial trials showed a large number of 'hops', a particle behavior defined as motion that occurs when the particle is making no contact with the topography. This behavior was observed by monitoring the contact force of the ball on the topography. Where the contact force is zero, the particle and topography are making no contact, indicating that the particle is in the air (Figure 2). The number of hops is determined by finding each time step where the contact force between the ball and the topography is greater than zero, and the time spent in the air is defined as the ratio between all data values where the wall contact force was zero and the total number of data values. The frequency of hops seen in this initial model using default parameters does not accurately represent debris flow mechanics, and resulted in an analysis of each parameter's influence on particle behavior.

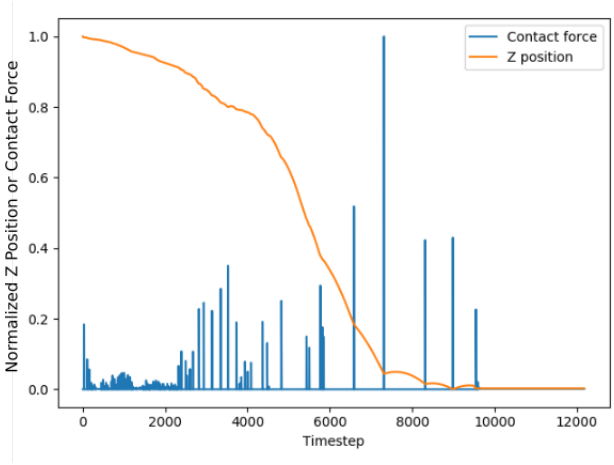

Figure 2: IfSAR derived digital elevation model used throughout the following tests as seen within PFC3D.

Results

After selecting which parameters to study, the sensitivity analysis was performed by holding all parameters constant except one. This one parameter is allowed to vary by the values in Tables 1 and 2.

Table 1: Default parameters for this study.

Contact stiffness (normal)	9.5e10 N/m
Contact stiffness (shear)	4.8e10 N/m
Friction	0.6
Damping Ratio	0.2
Density	2600 kg/m^3
Radius	5.0 m

Contact Stiffness

The normal contact stiffness was first varied in a range between 4.3e07 and 9.5e11 N/m (Table 2). Reducing the contact stiffness to 4.28e07 N/m and lower caused the particle to fall through the topography, so no lower values were tested. When the ball falls through the topography, the time step is

too large for the contact relationships to react and keep the ball on the surface. The ball then penetrates the surface, exits through the opposite side, and continues to fall under the force of gravity until it reaches the lower domain extent. Two trials were performed in every case, the only difference being the starting position. The trials are named by position on the x-axis of the model domain, with "525x" and "530x" corresponding to 525 m and 530 m, respectively. The number of hops, referred to as "hop count", shows a general trend of increasing logarithmically by the equation$y = 576.954 * \log x - 5324.039$, where y is hop count and x is normal stiffness, with contact stiffness in both trials (Figure 3a). To verify, the amount of time that the particle spent in the air was also calculated and plotted as a function of normal contact stiffness (Figure 3b). The number of hops made by the particle in trial 525x increased logarithmically from 2688 to 10137 while the number of hops made by the particle in trial 530x increased logarithmically from 4659 hops to 10,424 hops (Figure 4). The percentage of time steps spent in the air by the particle varied by 38.70% for trial 525x and 39.673% for trial 530x, increasing overall between 10^8 and 10^{11} N/m, then decreasing overall until 10^{12} N/m, but failed to show a monotonic trend. Vertical position as a function of time step was plotted as visual aid for the trajectory of each particle under different normal contact stiffness conditions for trial 525x (Figure 5), which shows that the largest hops occured where the particle impacted the relatively flat valley bottom at the outlet of the channel.

Table 2: Parameter ranges tested throughout this study.

Contact stiffness (normal)	4.2e07 - 9.5e11 N/m
Contact stiffness (shear)	4.8e06 - 4.8e11 N/m
Friction	0.0 - 1.0
Damping Ratio	0.0 - 10.0
Density	2600 kg/m^3
Radius	5.0 m

In the case of shear contact stiffness, the parameter was varied from 4.8e06 N/m to 4.8e10 N/m. Across both trials, increasing the shear contact stiffness appears to quadratically increase the number of hops by the equation $y = 8.275e^{3x^2}$ (Figure 7). The percent time spent in the air increased gradually between contact stiffnesses of approximately 4.8e07 N/m and 4.8e10 N/m, then decreased rapidly between 10^{10} N/m and 10^{12} N/m. Between trials 525x and 530x, the percentage of time steps that the particle spent in the air varied by 24.97% in trial 525x and 20.993% in trial 530x (Figure 6b).

Friction

The friction coefficient of the particle was varied from 0 to 1 in steps of 0.1. The number of hops made by the particle in trial 525x appear to increase nonlinearly with increasing friction coefficient. In trial 530x, the number of hops appears to increase rapidly between friction coefficients 0.0 and 0.5, then decrease

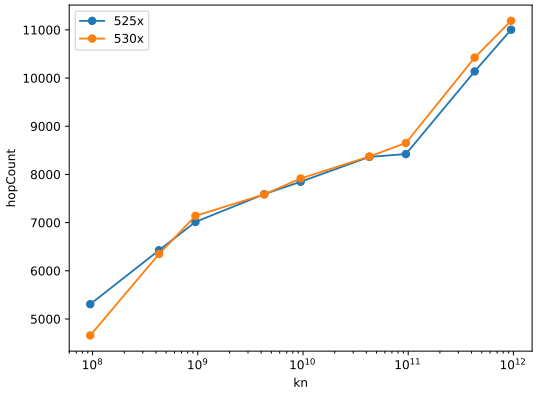

(a) Number of hops as a function of normal contact stiffness.

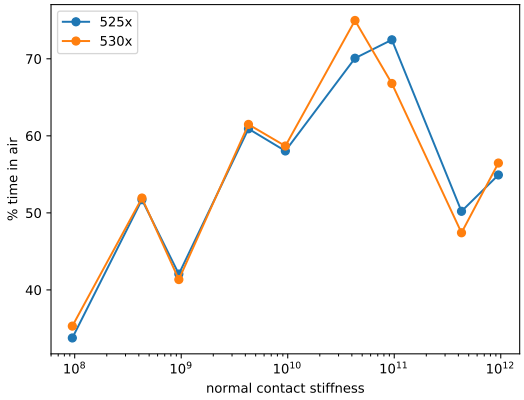

(b) Percent of timesteps spent in air by the particle.

Figure 3: Effects of varying normal contact stiffness values.

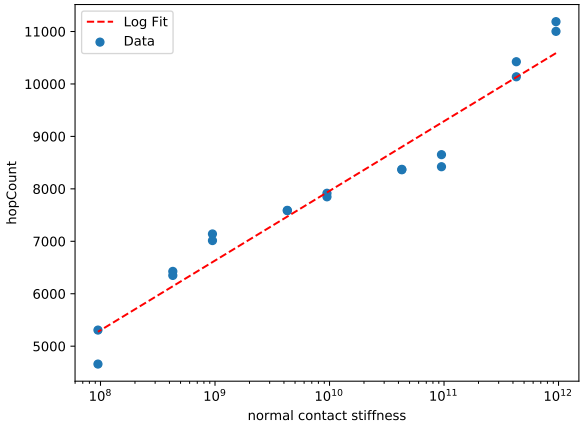

Figure 4: Affect of normal contact stiffness on the number of hops made by the particle with a logarithmic fit. Data composed of both trials.

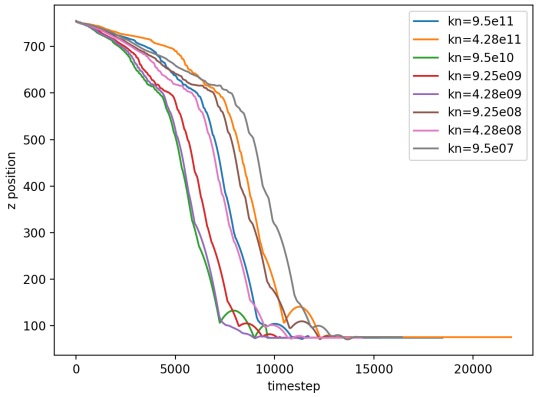

Figure 5: Vertical position as a function of time step with varying normal contact stiffness.

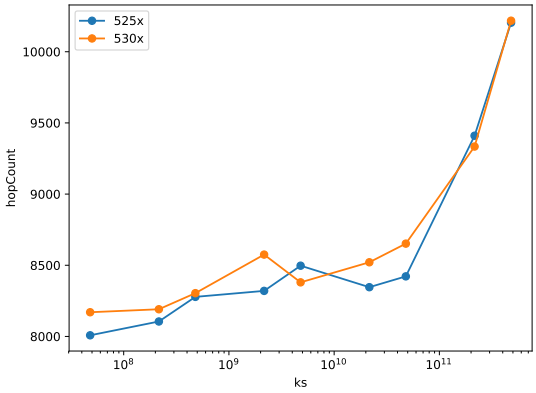

(a) Number of hops as a function of shear contact stiffness.

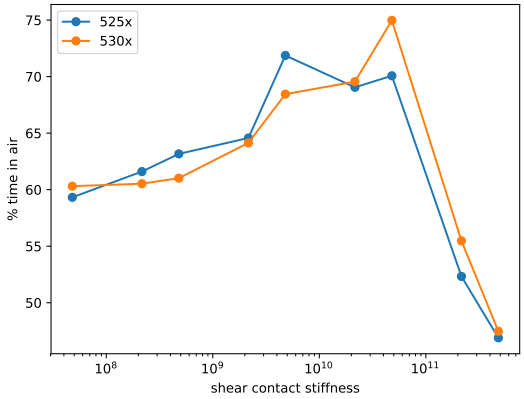

(b) Percent of timesteps spent in air by the particle.

Figure 6: Effects of varying shear contact stiffness values.

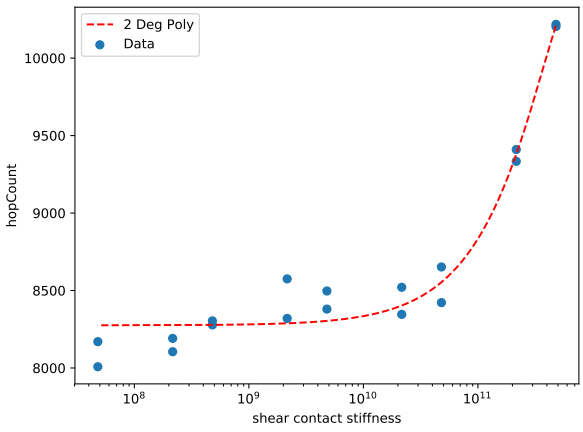

Figure 7: Affect of shear contact stiffness on the number of hops made by the particle with a quadratic fit. Data composed of both trials.

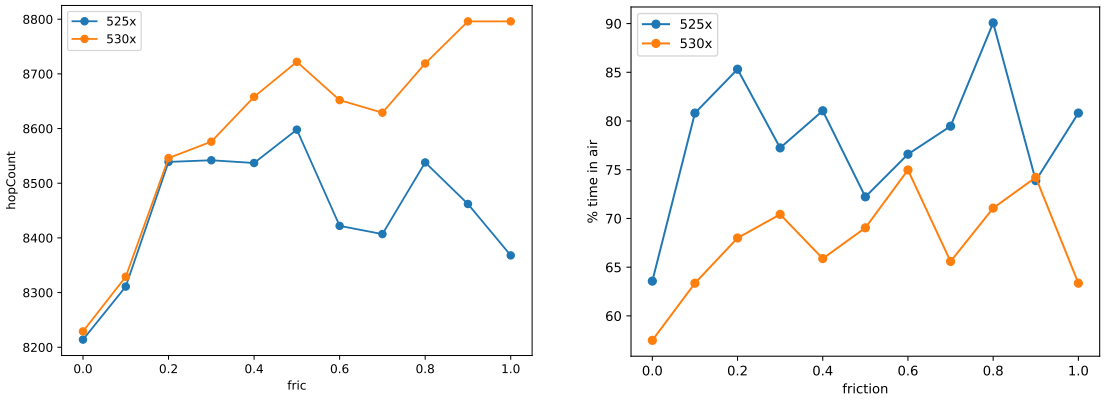

(a) Number of hops as a function of friction coefficient.

(b) Percent of timesteps spent in air by the particle.

Figure 8: Effects of varying friction coefficient.

gradually overall between friction coefficients 0.5 and 1.0. The percentage of time spent in the air by the particle increased gradually from μ=0 to 0.2, then became variable for μ> 0.2. In trial 525x percent time in the air varied by 26.51%, while it varied by 17.49% in trial 530x (Figure 8).

Damping

The damping ratio of the system was initially increased from 0 to 1 by steps of 0.1, then increased again to significantly larger numbers (2.0, 5.0, and 10.0) to find a clearer trend. The number of hops increases quadratically by equation from 7729 to 10541 in trial 525x and from 8540 to 10541 in trial 530x (Figure 10a), while the percentage of time in the air decreased by 79.78% in trial 525x, and by 87.549% for trial 530x (Figure 9b). This showed that the percent of time spent in the air by the particle decreases exponentially with increasing damping coefficient (Figure 10b). Vertical position as a function of time step for the particle under varying damping coefficient conditions of trial 525x has been provided for visual aid. As shown in Figure 9a, damping coefficients 2, 5, and 10 increased the time the ball spent in the colluvial hollow (Figure 1), and consequently raised the number of time steps necessary for the ball to enter the debris flow channel. Figure 11b shows the same data, but is zoomed in to show the differences between damping coefficients 0.0-1.0.

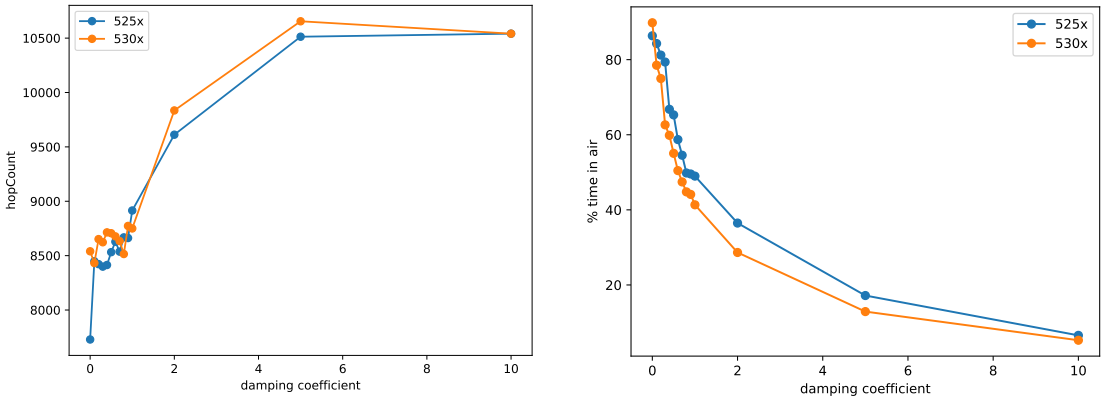

(a) Number of hops as a function of damping coefficient.

(b) Percent of timesteps spent in air by the particle.

Figure 9: Effects of varying damping coefficient values.

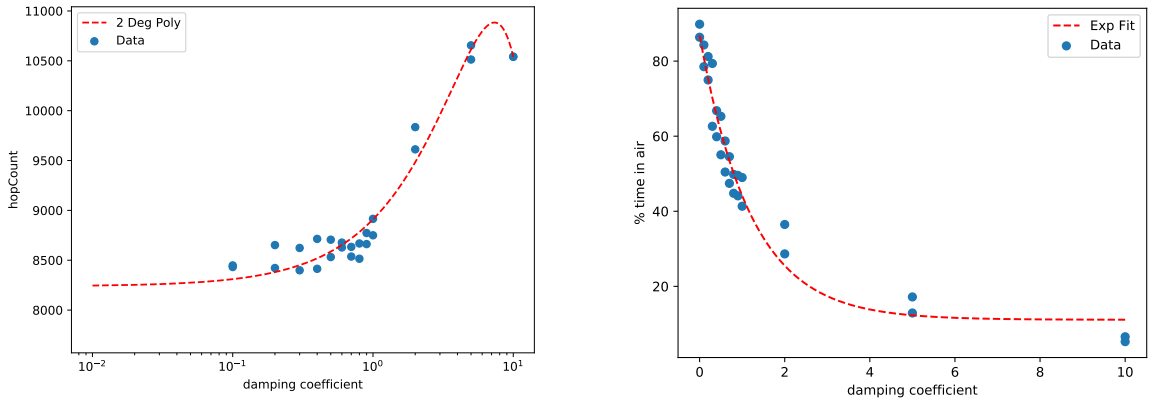

(a) Affect of damping coefficient on percentage of time steps spent in air by the particle with a quadratic fit.

(b) Affect of increasing damping coefficient on percentage of time spent in air by particle with an exponential fit.

Figure 10: Affect of damping coefficient on particle. Data composed of both trials.

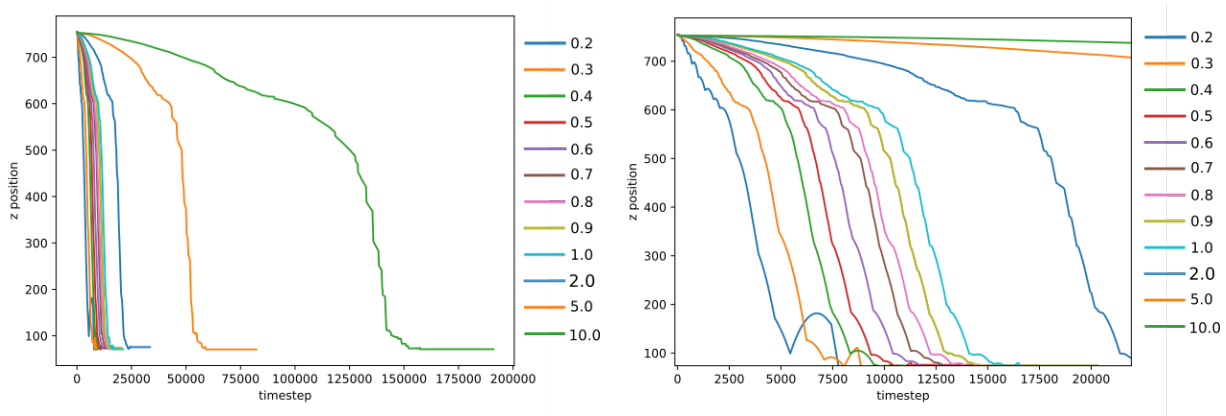

(a) Verticle position as a function of time step. Corresponds to trial 525x

(b) Verticle position as a function of time step, zoomed into trajectories of damping coefficients 0.0-1.0. Corresponds to trial 525x.

Figure 11: Vertical position as a function of time step with varying damping coefficients.

Discussion

The contact stiffness and bond strength, a parameter used to attach multiple particles to one another, are usually taken as the most significant parameters influencing precritical behavior of rock materials (Rojek et al., 2012). Working with only one particle, we have not experimented with bond strength. However, as seen in a comparison among Figures 3, 6, and 8, this work supports the importance of the normal contact stiffness in causing the large variation in the amount of time the particle spends in the air. A lower normal contact stiffness results in less time spent in the air, seemingly displaying more realistic debris flow behavior. It is a common choice to set the shear contact force equal to the normal contact force (Di Renzo and Di Maio, 2004), and the shear contact stiffness parameter is frequently based on the value of its normal counterpart (Malone and Xu, 2008).

It is worth discussing the peak observed in the percent time spent in the air by the particle while varying shear contact stiffness. A sharp decrease occurs at a shear contact stiffness of 10^{11} N/m, then drops significantly. This is due to the fact that the particle traveled to the bottom of the slope, then continued to travel until it reached the model domain. Unable to cross the model domain boundary, the particle sat still, resting on the topography. The peak in Figure 6b indicates that the particle reaches the model domain relatively quickly, then sits still for a longer period of time.

To relate this experiment to a larger, whole debris flow model, a smaller contact stiffness may reduce the particle-particle collision interactions resulting in a reduced energy transmission for each particle. For the Hsiaolin landslide, increasing the contact stiffness increased the energy transmission enough that the flow

deposition width increased to an appropriate amount. Digital elevation model subtraction was performed to determine a thickness distribution of the flow, and simulation thickness closely matched (within 5m) those results (Lo et al., 2011b).

In addition to the contact stiffness, the damping coefficient was one of the two most impactful parameters on the system, decreasing the amount of time the particle spends in the air as the coefficient itself is increased, and appears to have the same effect on both initial starting positions of the particle. For the Hsiaolin landslide, the damping coefficient was estimated based on the results of the restitution coefficient tests in the field using

$$\eta = \sqrt{\frac{(\ln(e))^2}{(\pi)^2 + (\ln(e))^2}} \tag{6}$$

an equation used by Chang et. al to estimate the damping ratio for rockfall collision (Chang et al., 2003). In a study on the Tsaoling landslide, the selected value could only be verified by back-analysis of the experimental data (Tang et al., 2009).

Friction does not appear to play a major role in the amount of time the particle spends in the air, however it is heavily relied on in tangential contacts (Malone and Xu, 2008). In the study of the Hsiaolin landslide, decreasing the friction coefficient increased the runout distance, and increasing the friction coefficient decreased the deposition width (Lo et al., 2011b). In the case of the Tsaoling landslide, various friction coefficients were tested in order to determine the most appropriate for the model, examining the behavior of values too high and too low until finding a range of friction coefficients that suited their study area (Tang et al., 2009).

Table 3: Optimized parameters for this study
*parameter varied throughout study

*Contact stiffness (normal)	9.5e8 N/m
*Contact stiffness (shear)	4.8e11 N/m
*Friction	0.6
*Damping Ratio	0.8
Density	2600 kg/m
Radius	5.0 m

An analysis of the sensitivity to various parameters used in discrete element modeling provides insight into calibrating future model runs. Varying the normal contact stiffness resulted in the number of hops increasing with contact stiffness. Tangential contact stiffness showed a similar behavior, but appeared to have a threshold in between 10^{10} N/m and 10^{11} N/m where the number of hops significantly increases while the percentage of time spent in the air by the particle significantly decreases. Similarly, increasing the damping coefficient increases the the number of hops for every trial, but decreases the

amount of time the particle spends in the air. Friction appears to have the least effect on the single particle behavior, showing variation by only 600 hops throughout both trials, and for a single particle is highly sensitive to the initial condition.

Based on the sensitivity analysis, results from each trial were used to optimize the parameters for a single particle traveling down the topography (Table 3). I defined the optimal parameter values as those which, when used in combination with each other, reduced the amount of time spent in the air by the particle to at most 20%. Using parameter ranges from other studies (Tang et al., 2009; Tamas, 2018; Zhou and Ng, 2010) (Table 4), my parameters were selected based on their position in these ranges combined with the behavioral results from this study.

Table 4: Parameter ranges from literature review.

Contact stiffness (normal)	8.0e3 - 9.5e10 N/m
Contact stiffness (shear)	4.0e3 - 4.8e10 N/m
Friction	0.5 - 0.6
Damping Ratio	0.2 - 0.7

Normal and shear contact stiffness were chosen largely for their effect on the percentage of time spent in the air by the particle in this study, and is confirmed appropriate by the ranges found in the literature review. Shear contact stiffness is an order of magnitude greater than the highest value in the range, but considering the spread of the range, I find the optimized value to be appropriate. The range for the friction coefficient was quite small, and considering its lack of trend in this study, was left at the default value. Similar to the shear contact stiffness parameter selected, the damping ratio parameter selected does not fall within the range of the literature review. The parameter selected, 0.8, is larger than the provided range, however determined an appropriate number based on the present study. By selecting contact stiffness that were similar to the default contact stiffnesses but provided the particle with less time spent in the air made particle behavior more predictable. Tweaking the damping coefficient, the second most impactful parameter, until reasonable results were obtained showed that the particle's time spent in the air can decrease from approximately 60% to 20%. Friction was not changed because of its lack of noticeable impact on the system.

Conclusion

In this study, the parameters decided on before running a simulation using the discrete element method were varied and analyzed for trends. Examining the sensitivity of these parameters allows us to to make an educated parameter selection when full scale debris flow models are ready to be run. The parameters

varied were contact stiffness (both normal and shear), friction, and damping coefficient. Starting with the parameters used in a study of the Hsiaolin landslide in Taiwan (Lo et al., 2011b), parameters were explored by sending a single particle down topography and collecting the number of hops it made and time spent in the air. The goal was to select parameters that would decrease the number of hops to reflect what is estimated to be more realistic debris flow behavior.

The number of hops made by the particle when increasing the normal contact stiffness shows a general trend of increasing logarithmically, but increasing shear contact stiffness, the number of hops increases quadratically. Increasing the friction coefficient showed no trend, but increasing the damping coefficient showed a quadratic increase in the number of hops.

Using parameters from other studies (Table 4) and comparing them with the trends observed in this study, parameters that provide more realistic debris flow behavior were able to be selected. Adjusting the parameters to the values shown in Table 3 decreased the amount of time spent in the air by the particle from 60% to 20%. These values provide a starting point for determining parameters in full-scale debris flow models that demonstrate debris flow runout.

*References

Y.-L. Chang, B.-L. Chu, and S.-S. Lin. Numerical simulation of gravel deposits using multi-circle granule model. *Journal of the Chinese Institute of Engineers*, 26(5):681–694, 2003.

J. Chen and H.-G. Matuttis. *Understanding the Discrete Element Method: Simulation of Non-Spherical Particles for Granular and Multi-body Systems*. Wiley, 2014.

A. Di Renzo and F. P. Di Maio. Comparison of contact-force models for the simulation of collisions in dem-based granular flow codes. *Chemical engineering science*, 59(3):525–541, 2004.

J.-J. Hung, C.-T. Lee, and M.-L. Lin. Tsao-ling rockslides, taiwan. *Catastrophic landslides: effects, occurrence, and mechanisms, Geol. Soc. Am. Rev. Eng. Geol*, 15:91–115, 2002.

A. C. Johnson, D. N. Swanston, and K. E. McGee. Landslide initiation, runout, and deposition within clearcuts and old-growth forests of alaska. *Journal of the American Water Resources Association*, 36(1):17–30, 2000. ISSN 1752-1688. doi: 10.1111/j.1752-1688.2000.tb04245.x. URL http://dx.doi.org/10.1111/j.1752-1688.2000.tb04245.x.

S. T. Lancaster, S. K. Hayes, and G. E. Grant. Effects of wood on debris flow runout in small mountain watersheds. *Water Resources Research*, 39(6):n/a–n/a, 2003. ISSN 1944-7973. doi: 10.1029/2001WR001227. URL http://dx.doi.org/10.1029/2001WR001227. 1168.

C.-M. Lo, m.-l. Lin, C.-L. Tang, and J.-C. Hu. A kinematic model of the hsiaolin landslide calibrated to the morphology of the landslide deposit. 123:22–39, 11 2011a.

C.-M. Lo, M.-L. Lin, C.-L. Tang, and J.-C. Hu. A kinematic model of the hsiaolin landslide calibrated to the morphology of the landslide deposit. *Engineering Geology*, 123(1-2):22–39, 2011b.

C.-Y. Lu, C.-L. Tang, Y.-C. Chan, J.-C. Hu, and C.-C. Chi. Forecasting landslide hazard by the 3d discrete element method: A case study of the unstable slope in the lushan hot spring district, central taiwan. *Engineering Geology*, 183:14–30, 2014.

K. F. Malone and B. H. Xu. Determination of contact parameters for discrete element method simulations of granular systems. *Particuology*, 6(6):521–528, 2008.

C. L. May. Debris flow characteristics associated with forest particlesin the central oregon coast range, m.s. thesis. page 121, 1998. ISSN 1752-1688. doi: 10.1111/j.1752-1688.2002.tb05549.x. URL http://dx.doi.org/10.1111/j.1752-1688.2002.tb05549.x.

C. L. May. Debris flows through different forest age classes in the central oregon coast range. *Journal of the American Water Resources Association*, 38(4):1097–1113, 2002. ISSN 1752-1688. doi: 10.1111/j.1752-1688.2002.tb05549.x. URL http://dx.doi.org/10.1111/j.1752-1688.2002.tb05549.x.

B. Mishra, T. Patra, and C. Murty. Mixing and segregation of particles in rotating drums using the discrete element method. In *Discrete Element Methods: Numerical Modeling of Discontinua*, pages 386–391. 2002.

J. S. of Fluid Mechanics. URL http://www.nagare.or.jp/.

J. Rojek, C. Labra, O. Su, and E. Oñate. Comparative study of different discrete element models and evaluation of equivalent micromechanical parameters. *International Journal of Solids and Structures*, 49(13):1497–1517, 2012.

K. Tamas. The role of bond and damping in the discrete element model of soil-sweep interaction. *Biosystems Engineering*, 169:57–70, 2018.

C.-L. Tang, J.-C. Hu, M.-L. Lin, J. Angelier, C.-Y. Lu, Y.-C. Chan, and H.-T. Chu. The tsaoling landslide triggered by the chi-chi earthquake, taiwan: insights from a discrete element simulation. *Engineering Geology*, 106(1-2):1–19, 2009.

G. G. Zhou and C. W. Ng. Numerical investigation of reverse segregation in debris flows by dem. *Granular Matter*, 12(5):507–516, 2010.